Digest Journal of Nanomaterials and Biostructures

Dig. J. Nanomater. Bios. **2026**; 21(4): 57277
https://doi.org/10.31083/DJNB57277

Original Research

Antimicrobial and Enzyme Inhibitory Activities of Silver Oxide and Copper Oxide Nanoparticles Green-Synthesized Using Plant Extracts

Farwa Anwar[1], Muhammad Asam Raza[1,*]

[1]Department of Chemistry, Hafiz Hayat Campus, University of Gujrat, 50700 Gujrat, Pakistan
*Correspondence: asamgcu@yahoo.com (Muhammad Asam Raza)
Academic Editor: Bong-Joong Kim
Submitted: 20 August 2026 Revised: 18 September 2026 Accepted: 1 October 2026 Published: 11 November 2026

Abstract

Background: Medicinal plants are a sustainable source of bioactive compounds for green synthesis of nanomaterials. Herein, silver oxide and copper oxide nanoparticles were green-synthesized using *Datura innoxia*, *Trianthema portulacastrum*, and *Carthamus oxyacantha* extracts. **Methods:** The formation of nanoparticles was confirmed by Fourier transform infrared spectroscopy, while their crystallinity, morphology, and elemental composition were probed by X-ray diffraction, scanning electron microscopy, and energy-dispersive X-ray spectroscopy, respectively. Activity against seven bacterial strains was assessed using the agar disc diffusion method. **Results:** Nanoparticles of both types exhibited antibacterial activities exceeding those of plant extracts. Copper oxide nanoparticles synthesized from *D. innoxia* extract and silver oxide nanoparticles synthesized from *C. oxyacantha* extract exhibited the highest activity against *Klebsiella pneumoniae* (inhibition zone diameter = 33.0 ± 1.1 mm) and 22.3 ± 1.2 mm (inhibition zone diameter), respectively. The nanoparticles were further assessed for acetylcholinesterase (AChE) and butyrylcholinesterase (BChE) inhibitory activities. Copper oxide nanoparticles synthesized using C. *oxyacantha* extract showed maximum AChE inhibition (95.8 ± 1.4%), and silver oxide nanoparticles synthesized using the same extract showed 78.5 ± 0.8% inhibition against BChE. **Conclusions:** These findings highlight the potential of plant extract–derived silver oxide and copper oxide nanoparticles as antimicrobials and enzyme inhibitors.

Keywords: green synthesis; metallic nanoparticles; enzyme inhibition; antibacterial activity; medicinal plants

1. Introduction

Nanotechnology represents a growing and innovative branch of modern science and technology, including the synthesis of compounds at the molecular and atomic scales [1]. This field involves an ultrafine particle called a nanoparticle, whose diameter ranges from 1–100 nm [2]. The size of 'nanoparticles' mainly depends upon the reduction method and surrounding medium. Nanoparticles find their application in biomedical and pharmaceutics, including biomarkers, diagnostics, cosmetics, immunology, bioimaging, antibacterial, drug delivery, genetic engineering, bio-remediation, energy production, and water treatment [3]. Metal-based nanoparticles of copper and gold have improved living standards; hence, they need to be biosynthesized extensively. Metal oxides (MOs) like titanium oxide and silicon oxide are mainly used in paints and also provide antibacterial, antifungal, and antialgal properties. Silver nanoparticles (AgNPs) exhibit antimicrobial properties by direct binding with bacterial cell proteins and have hydrophobic properties with less toxic effects. These nanoparticles provide cosmeceutical as well as therapeutic effects on hair as well as skin and are used for the treatment of wrinkles, photoaging, and dark spots [4].

Nanoparticles can be synthesized using physical, chemical, and biological methods. Physical methods, such as laser ablation, physical vapor deposition, inert gas condensation, and high-energy ball milling, produce uniformly distributed nanoparticles without solvent contamination [5,6]. Chemical methods utilize reducing and stabilizing agents to convert metal ions into nanoparticles and prevent their agglomeration [7], with common techniques including sol-gel, hydrothermal, microwave-assisted, and solvothermal synthesis. Although physical and chemical approaches provide controlled nanoparticle synthesis, they often involve high costs, toxic chemicals, and environmentally hazardous byproducts [8]. In contrast, biological or green synthesis offers an eco-friendly, cost-effective, and sustainable alternative by employing microorganisms, biomolecules, or plant extracts as natural reducing [5] and stabilizing agents [9]. Plant-mediated synthesis has gained particular attention because phytochemicals such as flavonoids, phenolics, terpenoids, and alkaloids regulate nanoparticle nucleation and growth, producing nanoparticles of diverse sizes and morphologies depending on the plant species and synthesis conditions [10]. The particle size is strongly influenced by factors such as phytochemical composition, pH, temperature, reaction time, precursor concentration, and the extract-to-metal ion ratio [11]. Generally, smaller nanoparticles exhibit enhanced surface reactivity and superior biological activities, including antimicrobial [12,13], and anticancer [14]. *Trianthema portulacastrum* belongs to *Aizoaceae* and is located in semi-arid, subtropical, and tropical regions. *T. portulacastrum* is important for its antioxidant, hepatoprotective, diuretic, and anti-inflammatory

Copyright: © 2026 The Author(s). Published by IMR Press.
This is an open access article under the CC BY 4.0 license.

Publisher's Note: IMR Press stays neutral with regard to jurisdictional claims in published maps and institutional affiliations.

activities; it is employed to alleviate liver-related disorders and inflammatory conditions such as edema and jaundice, as well as for its antimicrobial, anthelmintic, and antipyretic activities. The pharmacological applications of *T. portulacastrum* are due to phytochemicals, including 72.98% terpenes, 35.69% monoterpenes, 6.54% diterpenes, and 30.75% sesquiterpenes. Furthermore, 27.5% hexahydrofarnesyl acetone, 12.3% verbenene, 2.8% 3-*p*-menthane, 1.9% *cis*-carvyl propanoate, 1.9% trans-*p*-mentha-2,8-dienol [15]. *Carthamus oxyacantha* belongs to the family *Asteraceae*, which is among the largest flowering plant families, consisting of 10,000 species and 1000 genera, spread over various areas of the world. *C. oxyacantha* is anciently used for its medicinal use against various diseases like typhoid, cough, swelling, cancer, anticoagulant effects, and disorders related to the heart and throat [16]. *C. oxyacantha* based medicine was found beneficial for swelling and pain associated with trauma, while flowers are used against jaundice and seeds are laxative. The flowers and seeds are rich in bioactive compounds such as serotonins, sterols, flavonoids, and carthamin. *Datura innoxia*, belongings to *Solanaceae*, was first found in Asia, Africa, Europe and Australia. Most important traditional and ethnopharmacological uses include sedative, demulcent, anti-asthmatic, anti-hemorrhoidal, expectorant, hypnotic, anti-tumor, and anesthetic. *D. innoxia was* found to be enriched in alkaloids such as tropane alkaloids (atropine, hyoscine and hyoscyamine) and also contains steroids and steroidal glycosides [17]. The present study was designed to evaluate the antimicrobial and enzyme inhibition potential of the green-synthesized metal oxide nanoparticles.

2. Materials and Methods

2.1 Chemicals and Reagents

Different chemicals were used for the preparation of silver- and copper-based plant nanoparticles, such as silver nitrate, copper acetate, ethanol (95%) and methanol (95%). The acetylcholinesterase, butyrylcholinesterase, DTNB (5,5′-dithiobis-(2-nitrobenzoic acid)), acetylthiocholine iodide substrate, butyrylthiocholine iodide substrate, sodium phosphate buffer, nutrient broth and agar medium were purchased from Sigma-Aldrich (St. Louis, USA). The microbial strains used in this study were isolated from soil and obtained from the Molecular Biology Laboratory, Department of Zoology, University of Gujrat, and the Institute of Industrial Biotechnology, Government College University, Lahore.

2.2 Collection of Plant Material and Extraction

Aerial parts (leaves) of three selected plants were collected from Punjab (Pakistan), identified by the Department of Botany (University of Gujrat). The material was carefully washed with distilled water (to remove debris) and then chopped (into smaller pieces) and ultimately ground to powder. The 20 grams of powdered leaf extract were mixed with 150 mL of the solvent system methanol: ethanol (2:8) in a 250 mL flask and extracted for 48 hours on shaking. This plant extract was filtered using filter paper (Whatman No. 1), then preserved at 4 ℃ in an airtight bottle covered with aluminum foil and placed in a refrigerator.

2.3 Synthesis of Metal-Based Nanoparticles

Three different medicinal plant extracts were used to prepare silver and copper nanoparticles. Silver nitrate (1.0 mM) and copper acetate (3.0 mM) solutions were used as sources of metal. After adding 150 mL of silver nitrate to 150 mL of plant extract with continuous stirring, the reaction mixture was incubated with orbital shaking. The solution changed color (from yellow-orange to black), which indicates silver-based nanoparticle synthesis. Similarly, the solution changed color (from blue to brown) when 150 mL copper acetate solution was added to 150 mL plant extract, indicating the formation of copper-based nanoparticles [18]. The nanoparticles were separated from the reaction mixture by centrifugation and repeatedly washed with distilled water. The nanoparticles were dried at 100 ℃ in an oven and calcined (200–400 ℃). The experimental workflow followed for the synthesis of silver oxide and copper oxide nanoparticles of the above selected plants is summarized in Fig. 1.

2.4 Antibacterial Activity

The antimicrobial activity of prepared silver oxide and copper oxide nanoparticles of plant extracts was performed against bacterial strains using the agar disc-diffusion method with minor modification [19]. The microbial strains (seven) used in this study were obtained from soil samples. The respective inoculum was used for antibacterial assay against Streptomycin as a standard. The nutrient agar medium was prepared using nutrient broth and agar-agar in 300 mL of distilled water. The medium was autoclaved under standard conditions. The sterilized medium was poured into sterilized Petri dishes under aseptic conditions. The plates were uniformly inoculated with the respective bacterial strains. Sterile discs were positioned on the surface of the medium; each disc was impregnated with 25 µL of the plant extract and metal oxide nanoparticles. After incubating the culture plates at 37 ℃ for 24 hours, the diameters of the inhibition zones were determined. Each experiment was performed three times.

2.5 Enzyme Inhibition Assay

Acetylcholinesterase (AChE) and butyrylcholinesterase (BChE) inhibitory activities were determined following the procedure by Ellman et al. [20] with some minor changes. For this purpose, 50 µL of the test extract was mixed with 100 µL of acetylcholinesterase or butyrylcholinesterase solution in a test tube. The reaction mixture was allowed to stand for 10 minutes to facilitate interaction between the enzyme and the test



Fig. 1. Scheme illustrating the synthetic method of plant-based metal oxide nanoparticles.

sample. Subsequently, 50 µL of acetylthiocholine iodide (for AChE) or butyrylthiocholine iodide (for BChE) was added as the substrate, followed by the addition of 50 µL of DTNB and 1 mL of phosphate buffer solution (pH 8.0). The reaction mixtures were then incubated in a water bath at 37 ℃ for 30 minutes. The intensity of the color developed was measured spectrophotometrically at 400 nm. The experiment was conducted thrice and the percentage inhibition of AChE and BChE was calculated using the following equation:

$$\%\text{Inhibition} = \frac{\text{Absorbance(blank)} - \text{Absorbance(test)}}{\text{Absorbance(blank)}} \times 100$$

3. Results

3.1 Fourier Transform Infrared Spectroscopy

Fourier transform infrared spectroscopy was employed to identify the phytochemical functional groups involved in the green synthesis and stabilization of silver oxide and copper oxide nanoparticles using *D. innoxia*, *T. portulacastrum*, and *C. oxyacantha* extracts. The comparative FTIR spectra of the plant extracts and their corresponding nanoparticles exhibited noticeable shifts in peak positions, changes in band intensities, and the emergence of metal–oxygen vibrations after nanoparticle synthesis. The FTIR spectra of all three plant extracts displayed a broad absorption band within the 3283–3323 cm^{-1} region, corresponding to O–H stretching vibrations of hydroxyl groups present in phenolic compounds, flavonoids, alcohols, and adsorbed water molecules. These hydroxyl-rich phytochemicals are well recognized as effective reducing agents during green nanoparticle synthesis. Similarly, absorption bands observed between 2936 and 2971 cm^{-1} were assigned to aliphatic C–H stretching vibrations of methyl ($–CH_3$) and methylene ($–CH_2$) groups. Strong absorption bands appearing in the 1620–1701 cm^{-1} region were attributed to carbonyl (C=O) stretching vibrations associated with amides, aldehydes, ketones and carboxylic acids. Furthermore, characteristic peaks within the 1037–1056 cm^{-1} region corresponded to C–O stretching vibrations of alcohols, esters, ethers, polysaccharides, and glycosides, indicating that oxygen-containing biomolecules also participated in the capping of the nanoparticles. Changes in FTIR spectra have been widely reported for biosynthesized metallic nanoparticles and are considered characteristic evidence of phytochemical-mediated nanoparticle formation [21]. An important observation common to all synthesized nanoparticles was the appearance of absorption bands in the low-wavenumber region, which are characteristic of metal–oxygen stretching vibrations. In *T. portulacastrum*, a distinct band was observed at approximately 877 cm^{-1} (Fig. 2), consistent with Ag–O vibrations reported for silver oxide nanoparticles [22]. In *C. oxyacantha*, Ag–O stretching was observed near 877 cm^{-1} [23], while Cu–O vibrations were detected within the characteristic range near 1600 cm^{-1} (Fig. 3), confirming the formation of copper oxide nanoparticles [24]. Likewise, copper oxide nanoparticles synthesized using *D. innoxia* displayed similar metal–oxygen bands, supporting the successful formation of crystalline copper oxide nanostructures (Fig. 4).

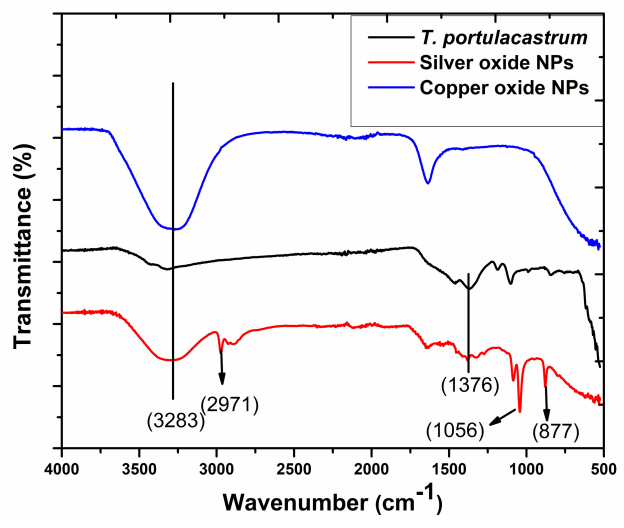


Fig. 2. FTIR spectra of silver oxide and copper oxide nanoparticles synthesized via *T. portulacastrum*.

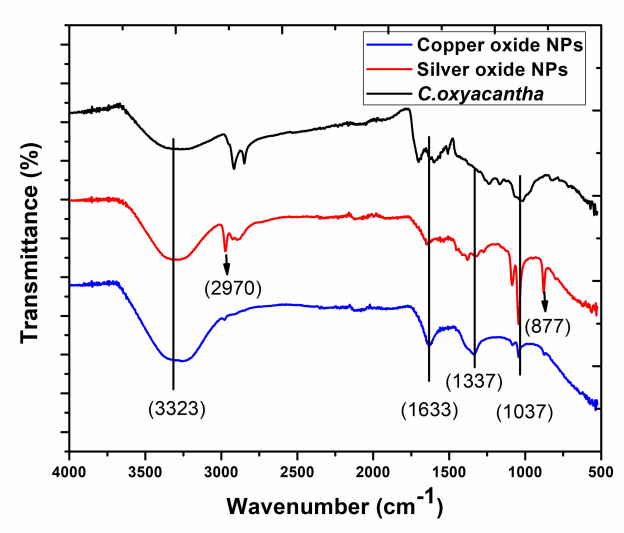


Fig. 3. FTIR spectra of silver oxide and copper oxide nanoparticles synthesized via *C. oxyacantha*.

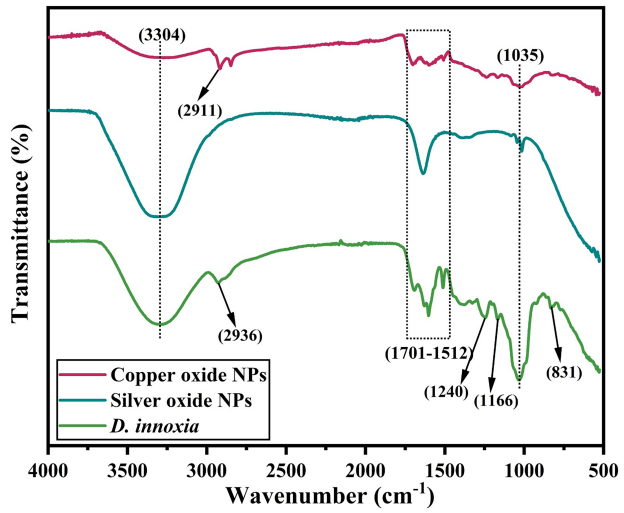


Fig. 4. FTIR spectra of silver oxide and copper oxide nanoparticles synthesized via *D. innoxia*.

3.2 Scanning Electron Microscopy Analysis

Scanning electron microscopy (SEM) micrographs demonstrated the successful green synthesis of predominantly spherical to quasi-spherical copper oxide nanoparticles with slight agglomeration, a characteristic feature of phytochemical-mediated synthesis (Fig. 5A,B,D,E,G,H). SEM analysis revealed average particle size diameters of 59.57 ± 2.16, 46.56 ± 2.51, and 28.11 ± 2.49 nm for *D. innoxia*, *T. portulacastrum*, and *C. oxyacantha*-mediated copper oxide nanoparticles, respectively. While energy-dispersive X-ray spectroscopy (EDX) further verified copper oxide formation by identifying copper as the predominant element (Fig. 5C,F,I). Oxygen was consistently detected alongside copper. The minor amounts of carbon, phosphorus, potassium, and chlorine reflected residual phytochemicals and naturally occurring mineral constituents from the plant extracts.

Similarly, SEM analysis revealed that the green-synthesized silver oxide nanoparticles were spherical, as shown in Fig. 6A,B,D,E,G,H. The average particle sizes were 24.71 ± 4.08, 55.98 ± 2.65, and 41.03 ± 2.38 nm for *D. innoxia*, *T. portulacastrum*, and *C. oxyacantha*, respectively. EDX analysis confirmed the successful formation of silver nanoparticles, with silver detected as the principal metallic element, as shown in Fig. 6C,F,I. The trace amounts of chlorine, potassium, magnesium, and phosphorus were attributed to residual plant-derived phytochemicals that likely acted as reducing, capping, and stabilizing agents during nanoparticle synthesis. Overall, the SEM and EDX analyses verified the successful green synthesis of silver oxide nanoparticles using all three plant extracts [25].

3.3 X-Ray Diffraction

The crystal structure and phase composition of the green-synthesized silver oxide and copper oxide nanoparticles were investigated by X-ray diffraction (XRD). The samples exhibited distinct diffraction peaks, indicating the formation of crystalline silver oxide and copper oxide nanoparticles through the green synthesis route. *D. innoxia*-mediated silver oxide nanoparticles showed characteristic reflections at 32.1° and 37.3°, indexed to the (111) and (200) crystallographic planes, respectively, attributed to a silver oxide phase (JCPDS No. 01-076-1489). In addition to the characteristic silver oxide reflections, weak diffraction peaks corresponding to the (110) and (032) planes were observed, which were assigned to an additional monoclinic Ag_3O_4 phase (JCPDS No. 00-040-1054). *C. oxyacantha*-mediated nanoparticles exhibited diffraction peaks at 27.6°, 37.1°, 44.4°, 54.5°, 57.1° and 64.1° corresponding to the (110), (11$\bar{2}$), (032), (20$\bar{2}$), (220) and (21$\bar{3}$) crystallographic planes, respectively, which are consistent with the monoclinic Ag_3O_4 phase (JCPDS No. 00-040-1054). Similarly, *T. portulacastrum*-mediated silver oxide nanoparticles displayed diffraction peaks at 26.7°, 32.8°, 44.3°, 54.5°, 57.0° and 64.2° indexed to the (110), (111), (032), (20$\bar{2}$), (220) and (21$\bar{3}$) crystallographic planes, respectively, with assignment to cubic Ag_2O (JCPDS No. 01-075-1532) as presented in Fig. 7.

The *D. innoxia*-mediated copper oxide nanoparticles exhibited characteristic diffraction peaks at 2θ values of 32.5°, 38.7°, 48.6°, and 61.4°, indexed to the (110), (111), (2$\bar{}$02), and (1$\bar{}$13) crystallographic planes, respectively, which are in good agreement with the monoclinic copper oxide phase (JCPDS No. 01-080-1916). Similarly, *C. oxyacantha*-mediated and *T. portulacastrum*-mediated samples exhibited reflections consistent with CuO at approximately 35.4°, 38.6°, 48.6°, 61.4°, and 74.9°, corresponding to the (1$\bar{}$11), (111), (2$\bar{}$02), (1$\bar{}$13), and (004) crystallographic planes, respectively. Additional diffraction peaks at 35.4°, 36.3°, 38.5°, 41.4°, 67.7° and 74.7°

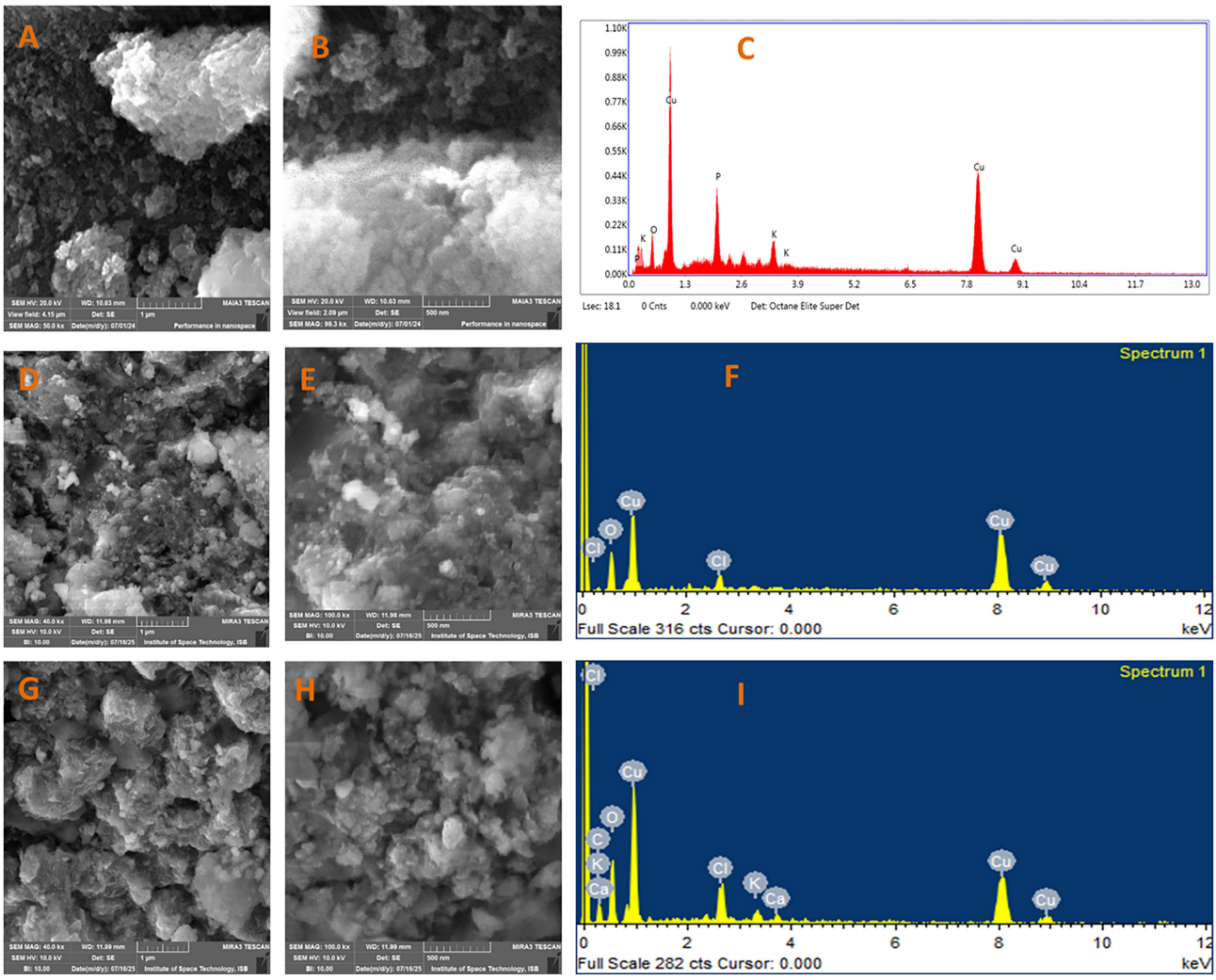


Fig. 5. SEM images (A and B: *D. innoxia*; D and E: *T. portulacastrum*; G and H: *C. oxyacantha*) and EDX spectra (C: *D. innoxia*; F: *T. portulacastrum* and I: *C. oxyacantha*) of green-synthesized copper oxide nanoparticles. SEM, scanning electron microscopy; EDX, energy-dispersive X-ray spectroscopy.

corresponding to the (022), (113), (004), (014), (026) and (242) crystallographic planes were obtained for *T. portulacastrum*-mediated copper oxide nanoparticles (JCPDS No. 01-078-1588) (Fig. 8).

The average crystallite size of the synthesized nanoparticles was determined from the broadening of selected XRD reflections using the Debye-Scherrer equation:

$$D = \frac{K\lambda}{\beta \cos(\theta)}$$

where D is the average crystallite size, K is the Scherrer constant (usually 0.9), λ is the wavelength of X-ray radiation (1.5406 Å for Cu Kα radiation), β is the full width at half maximum (FWHM) of a diffraction peak in radians and θ is the corresponding Bragg angle.

3.4 Antibacterial Potential

The antibacterial activity of the biosynthesized silver oxide and copper oxide nanoparticles was evaluated against seven bacterial strains using the agar disc diffusion method, with streptomycin serving as the positive control. The synthesized silver and copper oxide nanoparticles exhibited significant antibacterial activity against the tested bacterial strains, as demonstrated by the formation of distinct zones of inhibition around the discs. The clear inhibition zones confirmed the nanoparticles' ability to suppress bacterial growth, indicating their potent antibacterial activity. Overall, the green-synthesized nanoparticles displayed considerably higher antibacterial activity than their respective crude plant extracts, suggesting that the conversion of plant phytochemicals into metal oxide nanoparticles significantly enhanced their antimicrobial potential. Representative inhibition zones produced by *D. innoxia*-mediated silver oxide and copper oxide nanoparticles are presented in Fig. 9. The

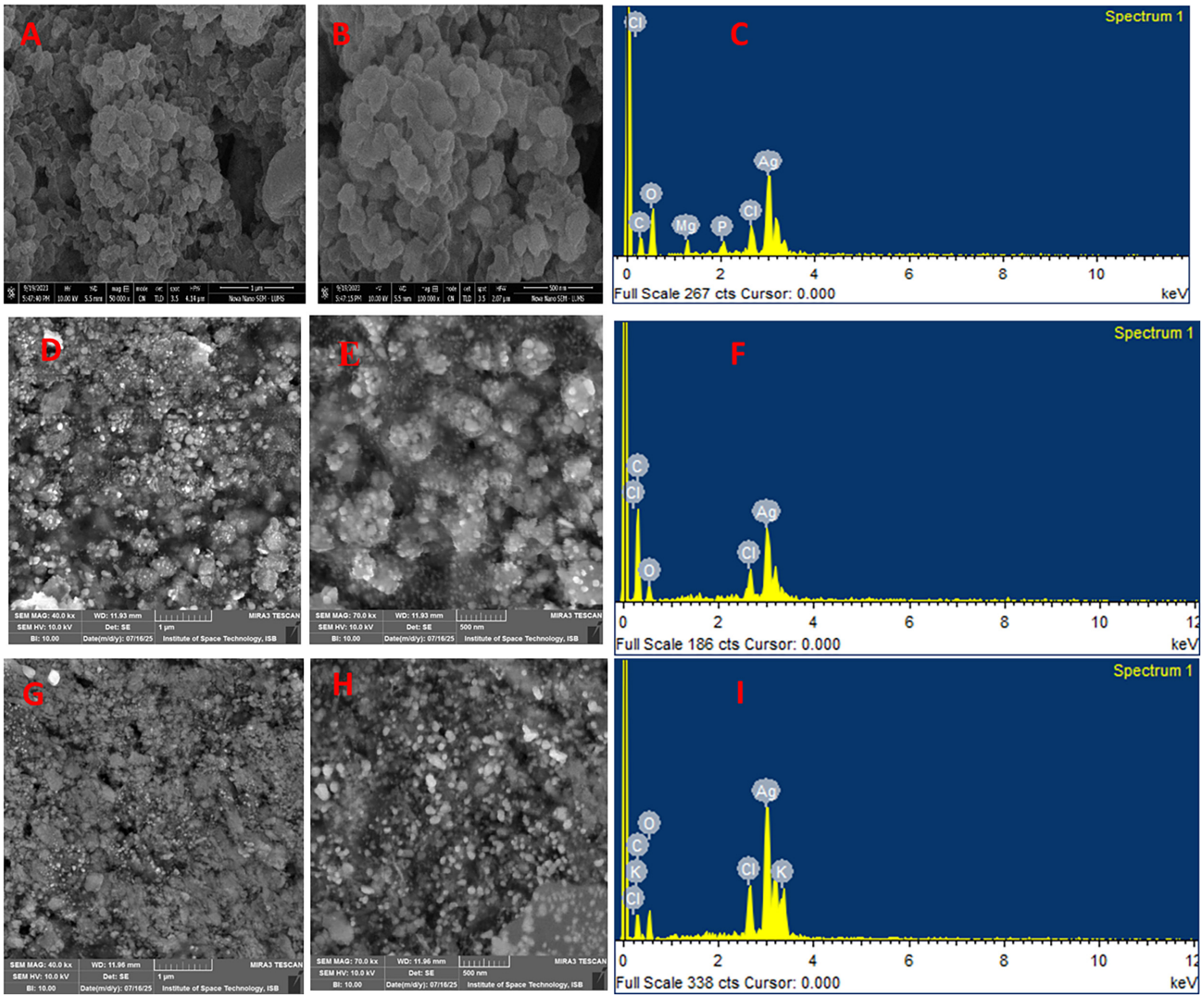


Fig. 6. SEM images (A and B: *D. innoxia*; D and E: *T. portulacastrum*; G and H: *C. oxyacantha*) and EDX spectra (C: *D. innoxia*; F: *T. portulacastrum* and I: *C. oxyacantha*) of green-synthesized silver oxide nanoparticles.

crude extract of *D. innoxia* exhibited antibacterial activity against *B. subtilis*, *H. salina*, *K. pneumoniae*, and *E. coli*, whereas the green-synthesized silver oxide nanoparticles demonstrated a pronounced antibacterial spectrum against all tested bacterial strains. The silver oxide nanoparticles showed activity of 12.1 ± 0.2 mm against *C. israelensis*, 14.4 ± 0.4 mm against *B. subtilis*, 21.2 ± 1.0 mm against *H. salina*, 16.5 ± 0.3 mm against *K. pneumoniae*, 15.9 ± 0.5 mm against *S. typhimurium*, and 21.2 ± 1.2 mm against *E. coli*. Among the tested microorganisms, *H. salina* and *E. coli* exhibited the highest susceptibility to the silver oxide nanoparticles, while *C. israelensis* showed the lowest sensitivity. Similarly, the copper oxide nanoparticles synthesized using *D. innoxia* also exhibited considerable antibacterial activity, with the strongest inhibitory effect against *K. pneumoniae*. Likewise, silver oxide nanoparticles synthesized from *C. oxyacantha* exhibited strong antibacterial activity against all tested bacterial strains (Fig. 10). The maximum zone of inhibition was observed against *K. pneumoniae* (22.3 ± 1.2 mm), indicating that this bacterium was highly susceptible to the synthesized nanoparticles. The enhanced antibacterial activity against *K. pneumoniae* may be attributed to the relatively permeable outer membrane of Gram-negative bacteria, which facilitates the interaction and penetration of silver oxide nanoparticles into the bacterial cell. In contrast, *B. subtilis* exhibited the lowest inhibition zone (15.0 ± 0.6 mm). The reduced antibacterial response of *B. subtilis* is likely due to its thick peptidoglycan layer, which acts as a structural barrier, limiting nanoparticle penetration and thereby reducing antibacterial effectiveness [26]. Copper oxide nanoparticles synthesized using *C. oxyacantha* also exhibited significant antibacterial activity against the tested bacterial strains. The highest zone of inhibition was observed against *S. aureus* (20.6 ± 0.9 mm), indicating that this bacterium was the most susceptible to the synthesized copper oxide nanopar-

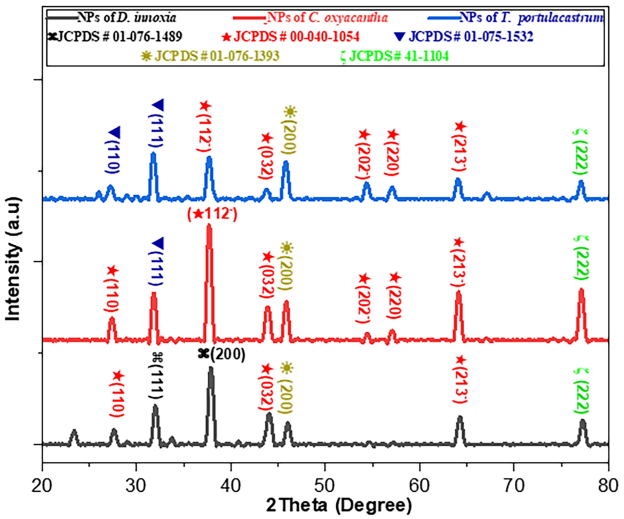


Fig. 7. XRD patterns of green-synthesized silver oxide nanoparticles using *D. innoxia*, *C. oxyacantha*, and *T. portulacastrum* extracts.

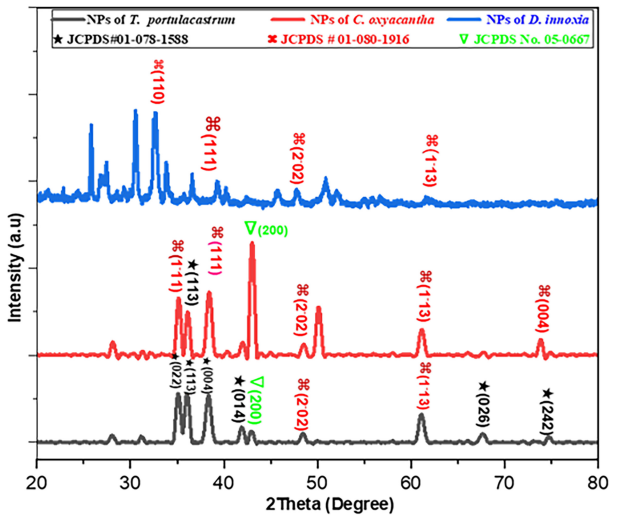


Fig. 8. XRD patterns of green-synthesized copper oxide nanoparticles from *D. innoxia*, *C. oxyacantha*, and *T. portulacastrum* extracts.

ticles (Fig. 10). In contrast, *K. pneumoniae* exhibited comparatively lower susceptibility, demonstrating a strain-dependent antibacterial response. Fig. 11 illustrates the antibacterial activity of *T. portulacastrum*-mediated silver oxide and copper oxide nanoparticles against the selected bacterial strains. Among the synthesized nanomaterials, silver oxide nanoparticles exhibited pronounced antibacterial efficacy, with the largest zone of inhibition recorded against *K. pneumoniae* (22.1 ± 1.0 mm) as shown in Table 1.

3.5 Enzymatic Inhibition Assay

The acetylcholinesterase and butyrylcholinesterase inhibitory activities of the plant extracts and their corresponding biosynthesized silver oxide and copper oxide nanoparticles were evaluated using Adam Kostelnik's method as previously described [27]. The inhibitory activities were expressed as percentage enzyme inhibition, and the comparative results are presented in Fig. 12. Among the investigated samples, *D. innoxia*-derived nanoparticles exhibited substantially higher cholinesterase inhibitory activity than the crude leaf extract. The *D. innoxia* extract inhibited BChE by 16.6 ± 0.3%, whereas the corresponding silver oxide and copper oxide nanoparticles exhibited significantly higher inhibition values of 60.8 ± 1.0 and 71.9 ± 1.1%, respectively. A similar trend was observed against AChE, with the crude extract showing 65.1 ± 0.6% inhibition, while silver oxide and copper oxide nanoparticles achieved 74.8 ± 0.9 and 82.1 ± 1.0%, respectively. These findings demonstrate that nanoparticle formation markedly enhanced the cholinesterase inhibitory potential of the plant extract. The silver oxide nanoparticles (*C. oxyacantha*) exhibited higher inhibitory activity (78.5 ± 0.8%) than copper oxide nanoparticles (44.8 ± 0.4%) against BChE. In contrast, copper oxide nanoparticles showed superior inhibition of AChE, 95.8 ± 1.4% inhibition with an IC_{50} of 73.2 µg/mL, whereas silver oxide nanoparticles inhibited AChE by 76.2 ± 0.6%. The enhanced inhibitory activity of the nanoparticle relative to the crude extract is also reported by Zahoor et al. 2026 [28].

Table 2 presents the comparative enzyme inhibition assay of the plant extract, silver oxide and copper oxide nanoparticles against AChE and BChE. The data indicate differences in percentage inhibition among the samples, suggesting that the green-synthesized nanoparticles exhibit enhanced cholinesterase inhibitory activity compared with the crude plant extract.

4. Discussion

In the FTIR spectrum, the variation in the position of metal–oxygen bands among different plant systems may be due to differences in the composition of secondary metabolites, nanoparticle size, crystallinity, morphology, and synthesis conditions, as previously reported [29]. The observed shifts in different functional groups, along with the appearance of characteristic Ag–O and Cu–O vibrations, clearly indicate the successful green synthesis of metal oxide nanoparticles. These findings are in close agreement with previous articles and further highlight the crucial role of plant metabolites in controlling nanoparticle nucleation, growth, and long-term stability [30,31,32]. In the XRD, a few low-intensity diffraction peaks corresponding to the (200) and (222) planes were compared with JCPDS card Nos. 01-076-1393 [33] and 41-1104 [34], respectively. These additional reflections suggest possible secondary components. The XRD patterns of the samples synthesized using *D. innoxia*, *C. oxyacantha*, and *T. portulacastrum* extracts confirm their crystalline nature, while additional reflections suggest the possible presence of sec-

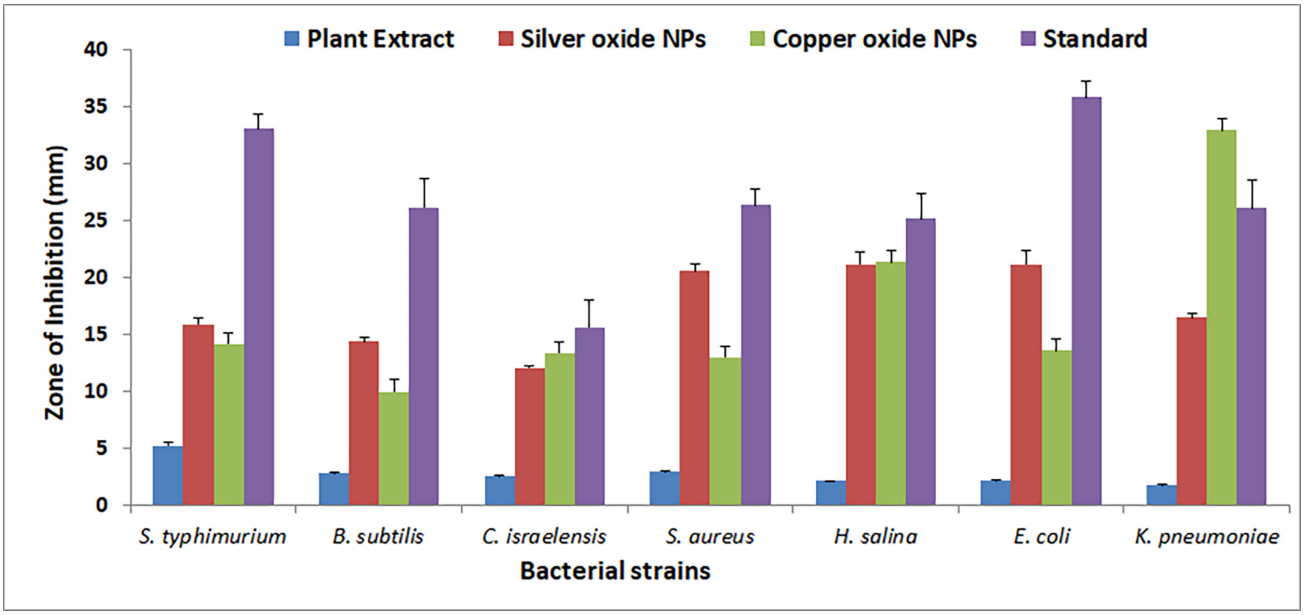


Fig. 9. Zones of inhibition exhibited by plant extract, green-synthesized silver oxide and copper oxide nanoparticles using *D. innoxia* leaf extract.

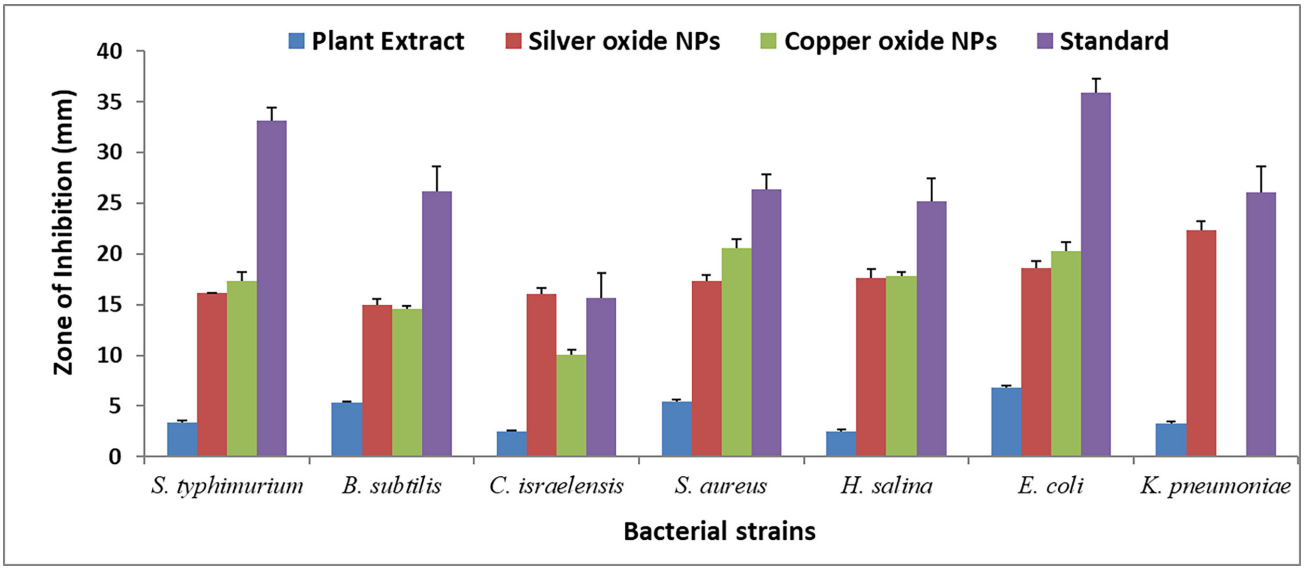


Fig. 10. Zones of inhibition exhibited by plant extract, green-synthesized silver oxide and copper oxide nanoparticles using *C. oxyacantha* leaf extract.

ondary crystalline phases. In addition to the characteristic copper oxide reflections, a diffraction peak was observed at 2θ ≈ 42.3°, indexed to the (200) lattice plane, which is consistent with cubic Cu_2O JCPDS No. 05-0667 [35] and may suggest the possible coexistence of CuO and Cu_2O. The XRD pattern of the D. innoxia-assistant copper oxide nanoparticles exhibited diffraction peaks at 2θ values of 25.8°, 27.4°, 30.6°, 33.7°, 36.5°, 40.2°, 45.6°, and 50.9°. The additional reflections may be associated with plant-derived crystalline residues or secondary phases formed during the green synthesis process. The diffraction peak observed at 36.5° was assigned and indexed to cubic cuprous oxide (Cu_2O) according to the JCPDS card No. 05-0667 [36]. These results indicate that the medicinal plant extracts mediated the formation of crystalline silver and copper oxide nanoparticles. The crystallite sizes of the silver oxide and copper oxide nanoparticles were calculated using the Scherrer equation. The sizes of the silver oxide nanoparticles synthesized using *D. innoxia*, *C. oxyacantha*, and *T. portulacastrum* extracts were 15.82, 18.79, and 15.90 nm, respectively. Similarly, the crystallite sizes of the copper oxide nanoparticles synthesized using *D. innoxia*, *C. oxyacantha*, and *T. portulacastrum* extracts were 13.17, 17.62, and 16.67 nm, respectively. These results in-

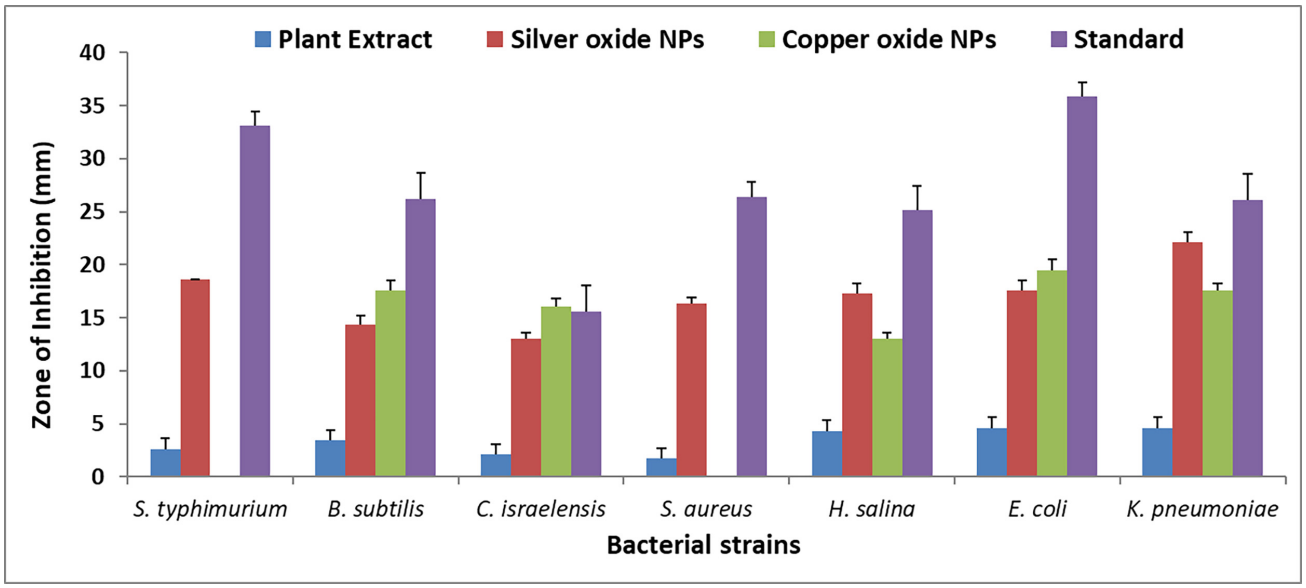


Fig. 11. Zones of inhibition exhibited by plant extract, green-synthesized silver oxide and copper oxide nanoparticles using *T. portulacastrum* leaf extract.

Table 1. Comparative antibacterial study of different bacterial strains.

Plant name		Zone of inhibition (mm)						
		S. typhimurium	*B. subtilis*	*C. israelensis*	*S. aureus*	*H. salina*	*E. coli*	*K. pneumoniae*
D. innoxia	Plant extract	5.2 ± 0.3	2.8 ± 0.05	2.5 ± 0.06	2.9 ± 0.08	2.1 ± 0.06	2.1 ± 0.09	1.7 ± 0.1
	Silver oxide NPs	15.9 ± 0.5	14.4 ± 0.4	12.1 ± 0.2	20.6 ± 0.6	21.2 ± 1.0	21.2 ± 1.2	16.5 ± 0.3
	Copper oxide NPs	14.2 ± 0.3	10.0 ± 0.1	13.4 ± 0.5	13.0 ± 0.3	21.4 ± 0.9	13.6 ± 0.6	33.0 ± 1.1
T. portulacastrum	Plant extract	2.6 ± 0.2	3.4 ± 0.2	2.1 ± 0.1	1.7 ± 0.2	4.3 ± 0.3	4.6 ± 0.6	4.6 ± 0.5
	Silver oxide NPs	18.6 ± 0.9	14.3 ± 0.6	13 ± 0.6	16.3 ± 0.9	17.3 ± 0.9	17.6 ± 0.9	22.1 ± 1.0
	Copper oxide NPs	Nil	17.6 ± 0.9	16.1 ± 0.7	Nil	13.0 ± 0.6	19.5 ± 1.0	17.6 ± 0.6
C. oxyacantha	Plant extract	3.4 ± 0.2	5.3 ± 0.1	2.5 ± 0.1	5.4 ± 0.2	2.5 ± 0.2	6.8 ± 0.2	3.3 ± 0.2
	Silver oxide NPs	16.1 ± 0.6	15 ± 0.6	16 ± 0.6	17.3 ± 0.9	17.6 ± 0.7	18.6 ± 0.9	22.3 ± 1.2
	Copper oxide NPs	17.3 ± 0.9	14.6 ± 0.3	10.1 ± 0.4	20.6 ± 0.9	17.8 ± 0.4	20.3 ± 0.9	Nil
	Standard	33.1 ± 1.3	26.1 ± 2.5	15.6 ± 2.4	26.4 ± 1.4	25.1 ± 2.2	35.8 ± 1.4	26.1 ± 2.5

NPs, nanoparticles; Nil, no activity.

Table 2. Comparative enzyme inhibition assay of plant extract, silver oxide and copper oxide nanoparticles.

Plant name	%age BChE inhibition			%age AChE inhibition		
	Plant Extract	Silver oxide NPs	Copper oxide NPs	Plant Extract	Silver oxide NPs	Copper oxide NPs
T. portulacastrum	43.1 ± 0.2	54.7 ± 0.3	60.1 ± 0.8	77.8 ± 0.8	79.7 ± 0.9	82.0 ± 1.0
C. oxyacantha	36.3 ± 0.4	78.5 ± 0.8	44.8 ± 0.4	58.1 ± 0.5	76.2 ± 0.6	95.8 ± 1.4
D. innoxia	16.6 ± 0.3	60.8 ± 1.0	71.9 ± 1.1	65.1 ± 0.6	74.8 ± 0.9	82.1 ± 1.0

dicated that the synthesized nanoparticles possessed crystallite dimensions within the nanometer range. The observed differences in crystallite size may be attributed to variations in the phytochemical composition of the plant extracts, which can influence nucleation, crystal growth, and stabilization during nanoparticle formation [11]. The antibacterial activity was tested using an *in vitro* model against tested bacterial starin. The substantial antibacterial activity indicates the strong bactericidal potential of the biosynthesized silver oxide nanoparticles. The increased susceptibility of *K. pneumoniae* may be attributed to the cell wall structure, which allows easier penetration of silver nanoparticles and silver ions [37,38]. Copper oxide nanoparticles biosynthesized using *T. portulacastrum* also exhibited considerable antibacterial activity and the highest inhibitory effect observed against *E. coli* (19.5 ± 1.0 mm). The enhanced antibacterial activity of the plant-mediated silver oxide and copper oxide nanoparticles may be attributed to their nanoscale dimensions, high surface-to-volume ratio, and reactive surface properties, which can promote interac-

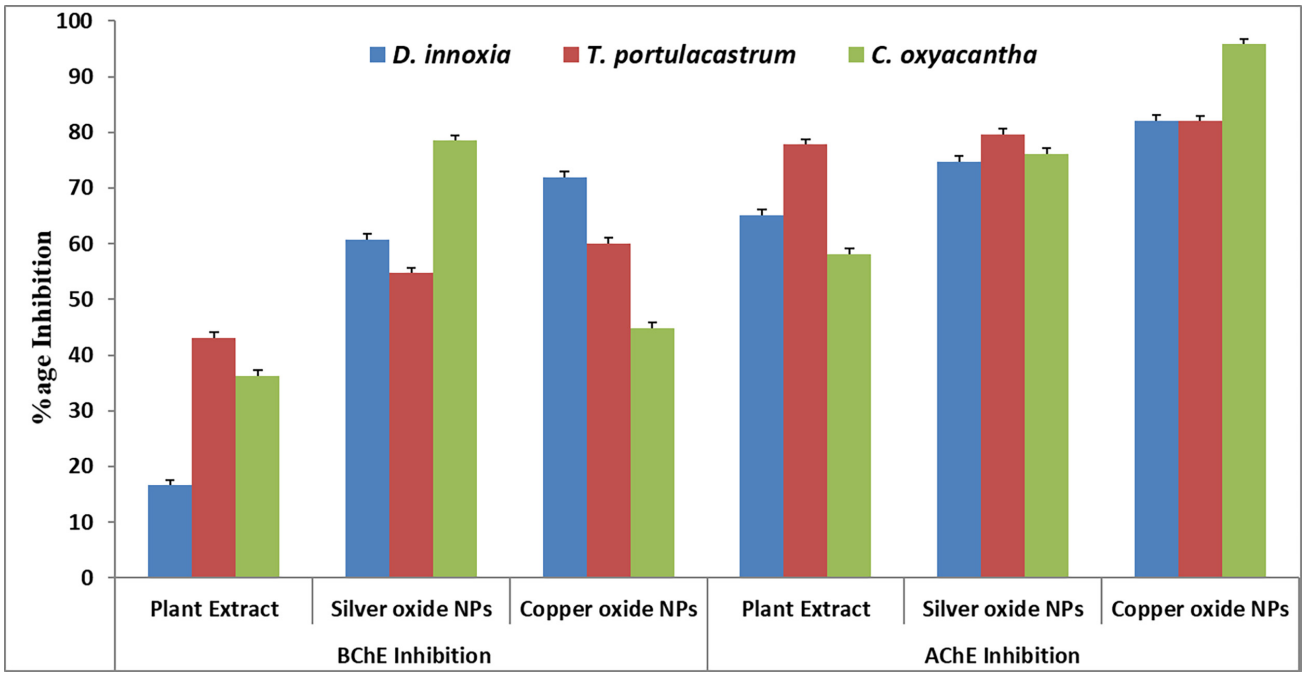


Fig. 12. BChE and AChE inhibition exhibited by *D. innoxia*, *C. oxyacantha* and *T. portulacastrum* leaf extract, green synthesized silver oxide and copper oxide nanoparticles.

tions with bacterial cell membranes. Previous studies suggest that copper oxide nanoparticles may exert antibacterial effects through membrane disruption and reactive oxygen species (ROS) generation [39], whereas silver-based nanoparticles have been associated with membrane damage, oxidative stress, and interference with cellular proteins and nucleic acids [40]. In the present study, it was noticed that synthesized silver oxide nanoparticles showed higher antimicrobial activity in comparison to copper-based metal nanoparticles and the original plant extract. The values are presented as mean ± standard error of three independent experiments. Phan et al., 2019 [41] conducted a comparative antibacterial study where copper composite had better bactericidal action against *B. subtilis* while silver had good bactericidal action against *E. coli.* Recently, research involving biogenic silver nanoparticles against bacteria haves been performed [42,43]. Both silver and copper oxide nanoparticles inhibited both enzymes, while copper oxide nanoparticles exhibited greater inhibitory activity especially against AChE than silver oxide nanoparticles. It was observed that against AChE, silver oxide nanoparticles produced 79.7 ± 0.9% inhibition, while copper oxide nanoparticles exhibited 82.0 ± 1.0% inhibition. The greater inhibition of AChE in most cases compared with BChE suggests a preferential interaction of the nanoparticles with the catalytic and peripheral anionic sites of acetylcholinesterase [44]. Overall, the results demonstrate that green synthesis significantly enhanced the cholinesterase inhibitory activity of all three medicinal plants. In most cases, the nanoparticles exhibited greater enzyme inhibition than the corresponding crude extracts, indicating that conversion into nanoscale metal oxides improves biological efficacy. This enhancement may be attributed to the high surface-to-volume ratio of the nanoparticles, improved bioavailability, increased adsorption onto enzyme surfaces, and the synergistic contribution of surface-bound phytochemicals acting as reducing and capping agents. Furthermore, the generally stronger inhibition observed against AChE than BChE suggests that nanoparticle–enzyme interactions are influenced by structural differences in the active-site architecture of the two cholinesterases, resulting in more favorable binding to AChE [45,46].

Limitations

The phytochemicals involved in the synthesis of the metal oxide nanoparticles were not characterized. The TEM analysis is also missing in the current study. Furthermore, the exact mechanism of the antibacterial study should be addressed in detail.

5. Conclusions

The aerial parts of *D. innoxia*, *T. portulacastrum* and *C. oxyacantha* were used to synthesize Ag and Cu based nanoparticle. The synthesized nanomaterials were characterized with advanced techniques, which confirmed the synthesis of the targeted nanoparticles. The SEM analysis revealed the nanosize of the plant-mediated materials. Furthermore, the EDX spectrum also confirmed the presence of the relevant metals in good percentages. It can also be observed from the results that silver- and copper-based plant nanoparticles are better antibacterial agents against

the tested strains compared to the plant extract, which may be due to their small size that helps in penetration of the cell membrane of the microbes. The synthesized materials were further evaluated against two enzymes of the esterase family, and it was shown that the plant-based silver oxide NPs showed better enzyme inhibition potential against BChE than copper oxide NPs, while in the case of AChE, copper oxide NPs depicted a better response than silver oxide nanoparticles. Overall, our findings suggest that silver and copper oxide NPs hold better potential against bacterial strains as well as against esterases. Furthermore, in silico studies should be conducted for these compounds against tested microbes as well as enzymes.

Availability of Data and Materials

The datasets used and analyzed during the current study are available from the corresponding author on reasonable request.

Author Contributions

FA and MAR have conducted the experimental work and narrated the initial draft, while MAR has supervised the whole project and finalized the draft. Both authors read and approved the final manuscript. Both authors have participated sufficiently in the work and agreed to be accountable for all aspects of the work.

Ethics Approval and Consent to Participate

Not applicable.

Acknowledgment

The authors are grateful to the University of Gujrat for providing research facilities.

Funding

This research received no external funding.

Conflicts of Interest

The authors declare no conflicts of interest.

References

[1] Khan I, Saeed K, Khan I. Nanoparticles: Properties, applications and toxicities. Arabian Journal of Chemistry. 2019; 12: 908–931. https://doi.org/10.1016/j.arabjc.2017.05.011

[2] Jeevanandam J, Barhoum A, Chan YS, Dufresne A, Danquah MK. Review on nanoparticles and nanostructured materials: history, sources, toxicity and regulations. Beilstein Journal of Nanotechnology. 2018; 9: 1050–1074. https://doi.org/10.3762/bjnano.9.98

[3] Singh R, Nalwa HS. Medical applications of nanoparticles in biological imaging, cell labeling, antimicrobial agents, and anticancer nanodrugs. Journal of Biomedical Nanotechnology. 2011; 7: 489–503. https://doi.org/10.1166/jbn.2011.1324

[4] Kaul S, Gulati N, Verma D, Mukherjee S, Nagaich U. Role of Nanotechnology in Cosmeceuticals: A Review of Recent Advances. Journal of Pharmaceutics. 2018; 2018: 3420204. https://doi.org/10.1155/2018/3420204

[5] Dhand C, Dwivedi N, Loh XJ, Jie Ying AN, Verma NK, Beuerman RW, et al. Methods and strategies for the synthesis of diverse nanoparticles and their applications: a comprehensive overview. RSC Advances. 2015; 5: 105003–105037. https://doi.org/10.1039/c5ra19388e

[6] Vinukonda A, Bolledla N, Jadi RK, Chinthala R, Devadasu VR. Synthesis of nanoparticles using advanced techniques. Next Nanotechnology. 2025; 8: 100169. https://doi.org/10.1016/j.nxnano.2025.100169

[7] Oliveira MM, Ugarte D, Zanchet D, Zarbin AJG. Influence of synthetic parameters on the size, structure, and stability of dodecanethiol-stabilized silver nanoparticles. Journal of Colloid and Interface Science. 2005; 292: 429–435. https://doi.org/10.1016/j.jcis.2005.05.068

[8] Sandhu ZA, Kaina, Ashraf S, Farwa U, Ashraf A, Ghaffar S, et al. Transition Metal Oxides as Photocatalysis Environmental Remediation for Organic Dyes: A Systematic Review. Journal of Chemistry. 2026; 6909960.

[9] Rónavári A, Igaz N, Adamecz DI, Szerencsés B, Molnar C, Kónya Z, et al. Green Silver and Gold Nanoparticles: Biological Synthesis Approaches and Potentials for Biomedical Applications. Molecules (Basel, Switzerland). 2021; 26: 844. https://doi.org/10.3390/molecules26040844

[10] El-Seedi HR, El-Shabasy RM, Khalifa SAM, Saeed A, Shah A, Shah R, et al. Metal nanoparticles fabricated by green chemistry using natural extracts: biosynthesis, mechanisms, and applications. RSC Advances. 2019; 9: 24539–24559. https://doi.org/10.1039/c9ra02225b

[11] Baba IA, Awe OB, Mustapha S, Abubakar MA, Abdulkareem AS, Tijani JO, et al. Influence of plant-derived extracts on the synthesis, physicochemical properties, and applications of metal and metal oxide nanoparticles. Hybrid Advances. 2026; 13: 100666. https://doi.org/10.1016/j.hybadv.2026.100666

[12] Staroń A, Długosz O. Antimicrobial properties of nanoparticles in the context of advantages and potential risks of their use. Journal of Environmental Science and Health. Part A, Toxic/-hazardous Substances & Environmental Engineering. 2021; 56: 680–693. https://doi.org/10.1080/10934529.2021.1917936

[13] Lallo da Silva B, Abuçafy MP, Berbel Manaia E, Oshiro Junior JA, Chiari-Andréo BG, Pietro RCR, et al. Relationship Between Structure And Antimicrobial Activity Of Zinc Oxide Nanoparticles: An Overview. International Journal of Nanomedicine. 2019; 14: 9395–9410. https://doi.org/10.2147/IJN.S216204

[14] Manonmani R., Sasikumar D., Manikandan S. Hybrid activities of biogenically enhanced Datura metel and copper oxide nanoparticles for photocatalytic and anti-cancer study. Ionics. 2024; 30: 7721–7739. https://doi.org/10.1007/s11581-024-05830-9

[15] Ilavenil KK, Senthilkumar V., Kasthuri A. Green synthesis of metal nanoparticles from three medicinal plants: a review of environmental and health applications. Discover Catalysis. 2025; 2: 3. https://doi.org/10.1007/s44344-025-00007-6

[16] Ikram M, Beshbishy AM, Kifayatullah M, Olukanni A, Zahoor M, Naeem M, et al. Chemotherapeutic Potential of Carthamus Oxycantha Root Extract as Antidiarrheal and In Vitro Antibacterial Activities. Antibiotics (Basel, Switzerland). 2020; 9: 226. https://doi.org/10.3390/antibiotics9050226

[17] Nasir B, Baig MW, Majid M, Ali SM, Khan MZI, Kazmi STB, et al. Preclinical anticancer studies on the ethyl acetate leaf extracts of Datura stramonium and Datura inoxia. BMC Complementary Medicine and Therapies. 2020; 20: 188. https://doi.org/10.1186/s12906-020-02975-8

[18] Disha SA, Sahadat Hossain M, Habib ML, Ahmed S. Green Synthesis of Nano-Sized Metal Oxides (Ag2O, CuO, ZnO, MgO, CaO, and TiO2) Using Plant Extract for a Sustainable Environ-

ment. Nano Select. 2025; 6: e70000. https://doi.org/10.1002/nano.70000
[19] Raza MA, Gull N, Lee SW, Seralathan KK, Park SH. Development of stimuli-responsive chitosan based hydrogels with anticancer efficacy, enhanced antibacterial characteristics, and applications for controlled release of benzocaine. Journal of Industrial and Engineering Chemistry. 2022; 109: 210–220. https://doi.org/10.1016/j.jiec.2022.02.004
[20] ELLMAN GL, COURTNEY KD, ANDRES V, Jr, FEATHERSTONE RM. A new and rapid colorimetric determination of acetylcholinesterase activity. Biochemical Pharmacology. 1961; 7: 88–95. https://doi.org/10.1016/0006-2952(61)90145-9
[21] Verma A, Bharadvaja N. Plant-Mediated Synthesis and Characterization of Silver and Copper Oxide Nanoparticles: Antibacterial and Heavy Metal Removal Activity. Journal of Cluster Science. 2022; 33: 1697–1712. https://doi.org/10.1007/s10876-021-02091-8
[22] El-Masry MM, Imam N.G. A comparative study between Ag-CuO/ epoxy and Mg-CuO/ epoxy hybrid nanocomposites: impressive electrical, mechanical and thermal properties. Journal of Materials Research and Technology. 2022; 18: 1784–1801. https://doi.org/10.1016/j.jmrt.2022.03.039
[23] Faryabi E, Sheikhhosseini E, Yahyazadehfar M. Iron ore pellets based-Ag2O nanoparticles as efficient Bi-functional heterogeneous catalyst for the synthesis tetrahydrobenzo[α]xanthens in green media. Frontiers in Chemistry. 2025; 13: 1413080. https://doi.org/10.3389/fchem.2025.1413080
[24] Ejeta BA, Aaga GF, Fereja WM, Mengesha B. Biofabrication of highly effective and easily regenerated CuO nanoparticles as adsorbents for Congo red and malachite green removal. Scientific Reports. 2024; 14: 24116. https://doi.org/10.1038/s41598-024-74974-5
[25] Singh AK, Raykar VS. Microwave synthesis of silver nanofluids with polyvinylpyrrolidone (PVP) and their transport properties. Colloid and Polymer Science. 2008; 286: 1667–1673. https://doi.org/10.1007/s00396-008-1932-9
[26] Rai M, Yadav A, Gade A. Silver nanoparticles as a new generation of antimicrobials. Biotechnology Advances. 2009; 27: 76–83. https://doi.org/10.1016/j.biotechadv.2008.09.002
[27] Kostelnik A, Pohanka M. Inhibition of Acetylcholinesterase and Butyrylcholinesterase by a Plant Secondary Metabolite Boldine. BioMed Research International. 2018; 2018: 9634349. https://doi.org/10.1155/2018/9634349
[28] Zahoor M, Khan S, Khan RS, Islam NU, Ikram M, Alotaibi A. Antioxidant, antimicrobial, and anticholinesterase activities of A. nitida leaf extract mediated silver nanoparticles. Scientific Reports. 2026; 18918.
[29] Siddiqi KS, Husen A. Current status of plant metabolite-based fabrication of copper/copper oxide nanoparticles and their applications: a review. Biomaterials Research. 2020; 24: 11. https://doi.org/10.1186/s40824-020-00188-1
[30] Iravani S. Green synthesis of metal nanoparticles using plants. Green Chemistry. 2011; 13: 2638. https://doi.org/10.1039/c1gc15386b
[31] Ahmed S, Ahmad M, Swami BL, Ikram S. A review on plants extract mediated synthesis of silver nanoparticles for antimicrobial applications: A green expertise. Journal of Advanced Research. 2016; 7: 17–28. https://doi.org/10.1016/j.jare.2015.02.007
[32] Mittal AK, Chisti Y, Banerjee UC. Synthesis of metallic nanoparticles using plant extracts. Biotechnology Advances. 2013; 31: 346–356. https://doi.org/10.1016/j.biotechadv.2013.01.003
[33] Bogireddy NKR, El Hachimi AG, Mejia YR, Kesarla MK, Varma RS, Becerra RH, et al. Pyridinic N anchored Ag and Au hybrids for detoxification of organic pollutants. Npj Clean Water. 2022; 5: 40. https://doi.org/10.1038/s41545-022-00187-w
[34] Fang H, Wang J, Shi S. Enhanced visible-light photocatalytic degradation of methylene blue via a ternary Ag2O@CuFe2O4@g-C3N4 Z-scheme heterojunction with synergistic Fenton-like reactivity for sustainable water remediation. RSC Advances. 2025; 15: 39909–39918. https://doi.org/10.1039/d5ra02882e
[35] Mikami K, Kido Y, Akaishi Y, Quitain A, Kida T. Synthesis of Cu_2O/CuO Nanocrystals and Their Application to H_2S Sensing. Sensors (Basel, Switzerland). 2019; 19: 211. https://doi.org/10.3390/s19010211
[36] Jiang X, Zhang M, Shi S, He G, Song X, Sun Z. Microstructure and optical properties of nanocrystalline Cu2O thin films prepared by electrodeposition. Nanoscale Research Letters. 2014; 9: 219. https://doi.org/10.1186/1556-276X-9-219
[37] Alshamari YMG, Alkhathlan HZ, Karuppiah P, Khan M, Danish EY, Aqel A, et al. Structural analysis and antimicrobial assessment of bioinspired silver nanoparticles from Ferula communis. Scientific Reports. 2025; 16: 3434. https://doi.org/10.1038/s41598-025-33436-2
[38] Shukla K, Giri B, Dwivede R. Efficient synthesis of plant-mediated silver nanoparticles and their screening for antimicrobial activity. Plant Science Today. 2017; 4: 143–150. https://doi.org/10.14719/pst.2017.4.3.328
[39] Meghana S, Kabra P, Chakraborty S, Padmavathy N. Understanding the pathway of antibacterial activity of copper oxide nanoparticles. RSC Advances. 2015; 5: 12293–12299. https://doi.org/10.1039/c4ra12163e
[40] Tripathi N, Goshisht MK. Recent Advances and Mechanistic Insights into Antibacterial Activity, Antibiofilm Activity, and Cytotoxicity of Silver Nanoparticles. ACS Applied Bio Materials. 2022; 5: 1391–1463. https://doi.org/10.1021/acsabm.2c00014
[41] Phan DN, Dorjjugder N, Khan MQ, Saito Y, Taguchi G, Lee H, et al. Synthesis and attachment of silver and copper nanoparticles on cellulose nanofibers and comparative antibacterial study. Cellulose. 2019; 26: 6629–6640. https://doi.org/10.1007/s10570-019-02542-6
[42] Bindhu MR, Umadevi M, Esmail GA, Al-Dhabi NA, Arasu MV. Green synthesis and characterization of silver nanoparticles from Moringa oleifera flower and assessment of antimicrobial and sensing properties. Journal of Photochemistry and Photobiology. B, Biology. 2020; 205: 111836. https://doi.org/10.1016/j.jphotobiol.2020.111836
[43] Maghimaa M, Alharbi SA. Green synthesis of silver nanoparticles from Curcuma longa L. and coating on the cotton fabrics for antimicrobial applications and wound healing activity. Journal of Photochemistry and Photobiology. B, Biology. 2020; 204: 111806. https://doi.org/10.1016/j.jphotobiol.2020.111806
[44] Colletier JP, Fournier D, Greenblatt HM, Stojan J, Sussman JL, Zaccai G, et al. Structural insights into substrate traffic and inhibition in acetylcholinesterase. The EMBO Journal. 2006; 25: 2746–2756. https://doi.org/10.1038/sj.emboj.7601175
[45] Liu Y, Yan B, Winkler DA, Fu J, Zhang A. Competitive Inhibition Mechanism of Acetylcholinesterase without Catalytic Active Site Interaction: Study on Functionalized C60 Nanoparticles via in Vitro and in Silico Assays. ACS Applied Materials & Interfaces. 2017; 9: 18626–18638. https://doi.org/10.1021/acsami.7b05459
[46] Fang L, Pan Y, Muzyka JL, Zhan CG. Active site gating and substrate specificity of butyrylcholinesterase and acetylcholinesterase: insights from molecular dynamics simulations. The Journal of Physical Chemistry. B. 2011; 115: 8797–8805. https://doi.org/10.1021/jp112030p